Fe-substituted indium thiospinels: New intermediate band semiconductors with better absorption of solar energy

Ping Chen,[1] Haijie Chen,[1] Mingsheng Qin,[1] Chongyin Yang,[1] Wei Zhao,[1] Yufeng Liu,[1] Wenqing Zhang,[1] and Fuqiang Huang[1,2,a)]
[1]*CAS Key Laboratory of Materials for Energy Conversion, Shanghai Institute of Ceramics, Chinese Academy of Sciences, Shanghai 200050, China*
[2]*Beijing National Laboratory for Molecular Sciences and State Key Laboratory of Rare Earth Materials Chemistry and Applications, College of Chemistry and Molecular Engineering, Peking University, Beijing 100871, China*

(Received 31 March 2013; accepted 16 May 2013; published online 3 June 2013)

The indium thiospinels In_2S_3 and $MgIn_2S_4$ are promising host for the intermediated band (IB) photovoltaic materials due to their ideal band gap value. Here, the optical properties and electronic structure of Fe-doped In_2S_3 and $MgIn_2S_4$ have been investigated. All the Fe-substituted semiconductors exhibit two additional absorption bands at about 0.7 and 1.25 eV, respectively. The results of first-principles calculations revealed that the Fe substituted at the octahedral In site would introduce a partially filled IB into the band gap. Thanks to the formation of IB, the Fe-substituted semiconductors have the ability to absorb the photons with energies below the band gap. With the wide-spectrum absorption of solar energy, these materials possess potential applications in photovoltaic domain. © *2013 AIP Publishing LLC*. [http://dx.doi.org/10.1063/1.4808352]

I. INTRODUCTION

The impurity photovoltaic and multiple band cells were considered as the third generation solar devices with ultra-high energy conversion efficiency.[1–4] For a conventional cell, the absorption layer is a single band semiconductor ($E_g \approx 1.0$–1.5 eV), which results in the wide-spectrum solar energy that cannot be completely utilized. The maximum efficiency of single-junction solar cell is 40% according to the Shockley-Queisser (SQ) theory.[5,6] How to break this limitation? In 1997, Luque and Martí theoretically proved that the solar cell with an intermediate band has a superior efficiency 63.1% which exceeded the SQ limit.[7] By increasing the numbers of intermediated band (IB), the limit efficiency can further reach to nearly 80%.[8] Inserting an IB into the gap of host semiconductor would provide new paths for light absorption which can generate more electron-hole pairs. While an IB material is applied in the solar cell, a higher photocurrent can be obtained, and the intermediate band solar cell (IBSC) has better efficiency than the single-junction cell.

Since the IB concept was proposed, many efforts have been done to search suitable materials and prepare practical devices. The quantum dot (QD) was first designed as the IB material, where the IB is derived from the confined electron states in the conduction band (CB).[9] The test of QD IBSC prototype devices confirmed the theoretical model and operation principle.[10,11] The highly mismatched alloys (HMA) $Ga_{1-x}In_xN_yAs_{1-y}$ (Ref. 12) and $Zn_{1-y}Mn_yO_xTe_{1-x}$ (Ref. 13) are also potential candidates for high-efficiency IB cell. For $Ga_{1-x}In_xN_yAs_{1-y}$, the N-substitution results in the splitting of conduction band, and optical transitions associated with these two subbands were observed; for $Zn_{1-y}Mn_yO_xTe_{1-x}$, oxygen-dopping leads to the formation of a localized state in the gap, and multiple optical transitions were detected. The band structure of HMA can be described by the band anti-crossing (BAC) model, and the following first-principles calculations[14–22] and empirical theoretical methods[23–26] are also used for understanding the observed experimental results. In recent work, the GaN_yAs_{1-y}-based multiband photovoltaic device was investigated, and the results demonstrated the feasibility by tailoring the band structure of HMA to fabricate the IBSC.[27]

In fact, the QD have weak photon absorption coefficients due to the lack of enough IB density of states (DOS).[28] To the best of our knowledge, the growing of HMA is performed usually by expensive epitaxy[12,29] or pulsed laser melted[13] technology because of the high mismatching between the dopant and host atoms. In order to overcome the defects of QD and HMA, researchers have also attempted to choose suitable impurity into bulk host semiconductor to form IB. Up to now, the first-principles electronic structure calculations have been widely applied to design and understand the bulk IB materials, such as Ti-doped GaAs or GaP,[30–33] Ti (Ref. 34) or Cr-doped[35] $CuGaS_2$, Cr-doped ZnS (Ref. 36) or ZnTe,[37,38] Ti or V-doped In_2S_3, $MgIn_2S_4$, or $CdIn_2S_4$,[39,40] Cr-doped AlP,[41] Ti-implanted Si,[42] chalcogens (S, Se, Te) and group III elements (B, Al)-coimplanted Si,[43] O-doped Cu_3BiS_3 (Ref. 44) or Cu_3SbS_3 (Ref. 45), and Cr-doped Cu_2ZnSnS_4.[46] It is worth noting that the V-doped In_2S_3 (Ref. 47) or SnS_2 (Ref. 48) and Cr (Ref. 49) or Sn-doped[50,51] $CuGaS_2$ IB semiconductors were synthesized based on the theoretical band structure calculations. These materials show a better absorption of solar spectrum due to the formation of IB which in accordance with the theoretical predictions. The recently reported Nb-doped In_2S_3 (Ref. 52) and N-doped Cu_2O

a)Author to whom correspondence should be addressed. Electronic mail: huangfq@mail.sic.ac.cn.

(Ref. 53) exhibit two absorptions below the band gap, which were considered as promising IB materials, although no band calculations have been done for these systems.

The In_2S_3 is an important material for photovoltaic applications due to its stability, non-toxicity, and superior optoelectronic characteristics. In the high-efficiency Cd-free $CuIn_xGa_{1-x}Se_2$ (CIGS) thin film solar cells, In_2S_3 is used to replace the highly toxic CdS buffer layer.[54] The band gap of In_2S_3 is reported ranging from 1.85 to 2.2 eV,[55–57] which is close to the optimum value of the maximum efficiency IBSC. The $MgIn_2S_4$ possesses an experimental band gap ranging from the 2.1 to 2.28 eV,[58,59] and it is also an ideal value to act as a high-efficiency IB host ($E_g \approx 2.0$–2.5 eV).[7] Moreover, the $MgIn_2S_4$ belongs to the direct gap semiconductor, and the theoretical absorption coefficients can reach to 10^4–10^5 cm^{-1} in the visible light region.[40] By inserting the IB into the band gap of In_2S_3 and $MgIn_2S_4$, they could absorb the photons in visible and near-infrared region, and thus they are good candidates to act as promising host semiconductors for the IB materials.

In the present study, the Fe-substituted In_2S_3 and $MgIn_2S_4$ semiconductor were investigated as the IB materials both experimentally and theoretically. The synthesized materials were characterized by the X-ray diffractometry, energy-dispersive X-ray spectroscopy (EDX), X-ray photoelectron spectroscopy (XPS), and absorption spectrometry. The optical absorption measurements showed that the Fe-substituted compounds exhibited two additional sub-band absorptions. The theoretical electronic structure calculations based on the density functional theory also used to understand the occurrence of IB in these semiconductors. The nearly full solar spectrum absorption due to the formation of IB indicates that such a material possesses potential applications in photovoltaic area.

II. EXPERIMENT AND COMPUTATION

A. Experimental details and characterization

A series of $In_{2-x}Fe_xS_3$ ($x = 0.0$, 0.05, 0.1, 0.2) and $MgIn_{2-x}Fe_xS_4$ ($x = 0.0$, 0.05, 0.1) samples were synthesized by the high-temperature solid state reaction from the high purity elements (Mg (99.99%, Aladdin), In (99.999%, SinoReagent), Fe (99.99%, Aladdin), and S (99.999%, SinoReagent)). First, the stoichiometrically weighted reactants were sealed in a quartz tube, then heated slowly to the target temperature ($In_{2-x}Fe_xS_3$: 850 °C, $MgIn_{2-x}Fe_xS_4$: 750 °C), and held at this temperature for 24 h. Second, the obtained samples were ground, resealed in another quartz tube and heated to the target temperature for another 48 h before cooling to room temperature. Last, the powders were removed from the tubes and ground for characterization.

The X-ray diffraction (XRD) patterns were characterized using Cu $K\alpha$ radiation ($\lambda = 1.5406$ Å) on a Bruker D8 Focus X-ray diffractometer operating at 40 kV and 40 mA. The elemental analyses were taken on a JSM-6510 equipped with an EDX. The XPS were measured on an ESCALAB 250 spectrometer equipped with a monochromatic Al-$K\alpha$ X-ray source. All the binding energies were referenced to the C 1s peak (284.6 eV). The room temperature optical absorption spectra were measured on a TU-1901 ultraviolet-visible-near infrared (UV-Vis-NIR) spectrometer, and a packed $BaSO_4$ powder was used as the standard.

B. Density-functional theory (DFT) computational method

In order to study the effect of Fe dopant on the electronic properties of In_2S_3 and $MgIn_2S_4$, the first-principles computations based on DFT were performed using the Vienna Ab initio Simulation Package (VASP).[60,61] The local density approximation (LDA) is used to describe the exchange correlation functional, and projector augmented wave[62] (PAW) method has been used in the present work. The atomic electron configuration for Mg treats 2*p*, 3*s* state as valence state, and the others are described by 4*d*, 5*s*, 5*p* valence states for In, 3*d*, 4*s* valence states for Fe, 3*s*, 3*p* valence states for S, respectively. Here, the cutoff energy of plane wave was chosen at 350 eV. The relaxation of geometry optimization was performed by full relaxation of all internal atomic positions as well as unit cell volume and shape until the total energy changes within 10^{-5} eV/atom, and the Hellmann-Feynman force on all atomic sites was less than 0.01 eV/Å.

The In_2S_3 has three crystallographic modifications as a function of temperature: α, β, and γ phase.[63,64] The β phase has a defect spinel structure with indium vacancies ordered in the tetrahedral sites (space group: $I4_1/amd$). The In atoms locate at three different lattice positions: In1(8c), In2(16h), and In3(8e), and thus there are three kinds In-S polyhedral structures. The In1-S and In2-S are distorted octahedrons which linked with each other by a shared edge, as shown in Figure 1(a) (they are marked with blue polyhedrons and red polyhedrons, respectively). The tetrahedrons are separated from each other and centered by In3 (indicated by violet in Figure 1(a)), which is also distorted. At high temperature or dopped with other element, the cation vacancies are randomly distributed, and the structure undergoes a phase transition to the cubic α form (see Figure 1(b), space group: Fd-3m). In general, the α-In_2S_3 is considered as the same structure with the β phase except the cation vacancies disordered.[47] The present theoretical calculations were carried out using the tetragonal cell of β phase. An In atom was substituted by the Fe atom corresponding to the 3.125% dopant concentration ($In_{31}Fe_1S_{48}$).

The $MgIn_2S_4$ crystallize in the cubic spinel structure, where the Mg and In atoms are situated at the tetrahedral and octahedral sites, respectively (space group: Fd-3m, see Figure 1(c)). In the present calculations, the structural model was constructed on the direct spinel $MgIn_2S_4$ for simplicity. The conventional crystalline cell consists of 56 atoms, and the 6.25% dopant concentration is modeled by one Fe atom replacing one In atom ($Mg_8In_{15}Fe_1S_{32}$).

In the calculations of In_2S_3 system, the Brillouin zone integration has been performed with a gamma centered $4 \times 4 \times 1$ Monkhorst-Pack grids. For the Fe-doped $MgIn_2S_4$, gamma centered $4 \times 4 \times 4$ Monkhorst-Pack (MP) grids were used. In all calculations, the spin-polarization was considered. The total energy and DOS calculations were performed using tetrahedron method with Blöchel correction.

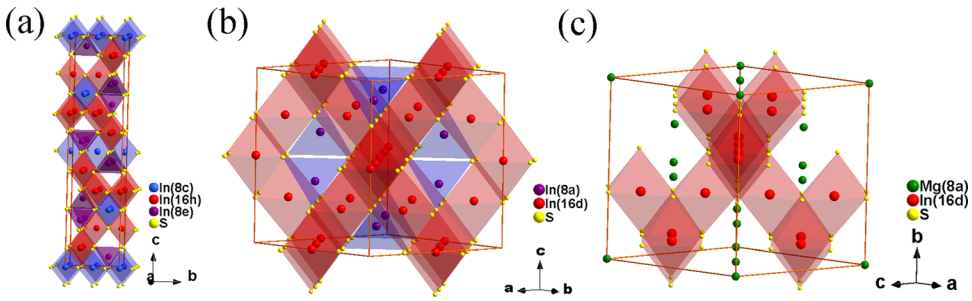

FIG. 1. The crystal structures of (a) β-In_2S_3 (tetragonal symmetry), (b) α-In_2S_3 (cubic symmetry), and (c) $MgIn_2S_4$, respectively.

III. RESULTS AND DISCUSSION

The synthesized $In_{2-x}Fe_xS_3$ and $MgIn_{2-x}Fe_xS_4$ powders were first characterized by the X-ray diffraction. Figure 2(a) shows the XRD patterns for the synthesized $In_{2-x}Fe_xS_3$ samples. The patterns of In_2S_3 and $In_{1.95}Fe_{0.05}S_3$ are similar to each other. All the peaks agree well with the standard card of tetrahedral β-In_2S_3 (JCPDS No. 25-0390), and no other impurity phase has been observed. With further increasing the concentration of Fe dopants ($In_{1.9}Fe_{0.1}S_3$ and $In_{1.8}Fe_{0.2}S_3$), the patterns can be indexed to the α-In_2S_3 phase (standard card: JCPDS No. 65-0459). As shown in Figure 2(a), the (004)-β, (112)-β, (008)-β, and (1013)-β peaks which can be used to distinguish the β and α phases, are indicated. The XRD structural analysis clearly evidenced that the In_2S_3 undergoes a phase transition from the ordered β to the disordered α phase. The driving force can be ascribed to the occurrence of chemical disorder while the substitution Fe for In. The phenomenon of structural transition also has been observed in the case of Al-doped In_2S_3.[65] Figure 2(b) shows the XRD patterns for the $MgIn_{2-x}Fe_xS_4$. All the diffraction peaks agree well with the standard card (JCPDS No. 31-0792), suggesting the purity of the obtained samples. The lattice parameters which fitted from the XRD patterns and the corresponding volumes are listed in Table I. The lattice parameters between the α and β-In_2S_3 can be described by the following formula: $a_\alpha \approx a_\beta \times \sqrt{2} \approx c_\beta/3$.[65] Thus the unit cell volume of them can have the relationship: $V_\alpha \approx V_\beta \times 2/3$. As seen from Table I, the crystal cell volumes decrease with respect to the addition of Fe dopants. It is reasonable because the effective ionic radius of Fe^{3+} (0.78 Å, 8-coordination) is smaller than that of In^{3+} (0.92 Å, 8-coordination).[66] The evolution of cell volume and lattice parameters indicate that the Fe ions are introduced into the semiconductor hosts lattice.

The compositional analysis for $In_{1.9}Fe_{0.1}S_3$ and $MgIn_{1.9}Fe_{0.1}S_4$ samples was investigated by the EDX. As depicted in Figure 3, the results show that the compositions of crystals are well matched with the nominal chemical elements. The signals of Fe element appear at 0.57 and 6.4 keV, respectively. The element mappings for two samples indicate that all elements including the Fe dopants are homogenous distribution without partial aggregation (not shown). The XPS has been used to determine the valence state of ions and also further confirm the chemical composition information of obtained sample. The XPS spectra of $In_{1.9}Fe_{0.1}S_3$ and $MgIn_{1.9}Fe_{0.1}S_4$ are presented in Figures 4(a) and 4(b), respectively. For $In_{1.9}Fe_{0.1}S_3$, the In $3d_{5/2}$ peak is 445.5 eV supporting the assignment of In^{3+}, and the S spectrum of $2p_{3/2}$ peak is 162.2 eV confirming the presence of anionic S atoms (see Figure 4(a)). In $MgIn_{1.9}Fe_{0.1}S_4$, the Mg 1s peak is recorded at 1305.0 eV which represents the Mg^{2+}. The In $3d_{5/2}$ peak is observed at 445.4 eV and S $2p_{3/2}$ peak is at 162.0 eV, respectively. In these two compounds, the small difference in the binding energy of In $3d_{5/2}$ and S $2p_{3/2}$ peak is derived from the different surrounding of ions. For the Fe spectra, the Fe $2p_{3/2}$ peak position is located at 709.2 eV for both the $In_{1.9}Fe_{0.1}S_3$ and $MgIn_{1.9}Fe_{0.1}S_4$. The satellite peak of Fe $2p_{3/2}$ is at 717.5 eV which is 8.3 eV higher than the main peak. The main differences between the Fe^{3+} and Fe^{2+} are the positions of Fe $2p_{3/2}$ peak and its satellite peak. For Fe^{3+} and Fe^{2+}, the difference between the Fe $2p_{3/2}$ peak and its associated satellite peak is 7.8 and 5.7 eV, respectively.[67] Therefore, it can conclude that the Fe atoms substitute the In positions which act as the trivalent dopant (Fe^{3+}, $3d^5$ configuration) to maintain the charges balance.

The absorption pattern is an efficient tool to investigate the optical properties and also detect the electronic structure information. Most importantly, the enhanced photon harvest is a crucial criterion to judge whether a material possesses a practical utility in photovoltaic area or not. Figure 5 shows the UV-Vis-NIR absorption patterns of the $In_{2-x}Fe_xS_3$

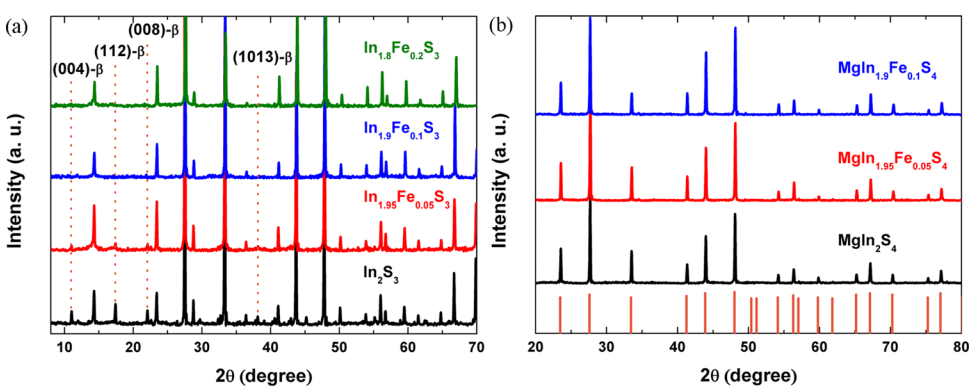

FIG. 2. The powder X-ray diffraction patterns of (a) $In_{2-x}Fe_xS_3$ and (b) $MgIn_{2-x}Fe_xS_4$, respectively.

TABLE I. The lattice parameters *a*, *c* (in Å) and corresponding crystal cell volumes V (in Å^3) for $In_{2-x}Fe_xS_3$ and $MgIn_{2-x}Fe_xS_4$ polycrystalline powders, respectively.

Nominal composition	*a*	*c*	*V*
In_2S_3	7.610	32.232	1866.62
$In_{1.95}Fe_{0.05}S_3$	7.601	32.220	1861.52
$In_{1.9}Fe_{0.1}S_3$	10.74		1858.25
$In_{1.8}Fe_{0.2}S_3$	10.715		1845.3
$MgIn_2S_4$	10.697		1224.01
$MgIn_{1.95}Fe_{0.05}S_4$	10.688		1220.93
$MgIn_{1.9}Fe_{0.1}S_4$	10.667		1213.74

(Figure 5(a)) and $MgIn_{2-x}Fe_xS_4$ (Figure 5(b)) powders. For the pure In_2S_3 and $MgIn_2S_4$ semiconductor, the strong absorption raises steeply about 1.8 eV and 2.0 eV, respectively, which correspond to the optical transition between the valence band VB and the CB. The optical gap of In_2S_3 was determined to be 1.85 eV from the Kubelka-Munk (K-M) transform function.[68] In contrast, the previously reported experimental values for the bulk or film In_2S_3 is ranging from 1.85 eV to 2.2 eV,[55–57] which may be derived from the structure effects, size effects, and also the difference of experimental technology. Hence, the obtained gap value is reasonable for the present In_2S_3 powder sample. For the $MgIn_2S_4$, the optical gap was determined to be 2.18 eV, which is in accordance with the previous reported experimental values.[58,59] When compared with the pure In_2S_3 and $MgIn_2S_4$, the absorptions of Fe-doped samples possess a significant enhancement at all light region. The optical absorption intensities also reveal the dependence on the Fe content. For each Fe-incorporated compound, two additional new absorptions at about 0.7 and 1.25 eV, which are distinctly different from the intrinsic band gap absorption, have been detected. Compared with the AM1.5G solar spectrum (the light yellow background in Figure 5), the Fe-substituted materials nearly absorb the photons in full spectrum region. The optical absorption behavior of Fe-doped In_2S_3 and $MgIn_2S_4$ is also very similar to the previous reported IB semiconductors, such as V-doped In_2S_3 (Ref. 47) or SnS_2,[48] Cr-doped $CuGaS_2$,[49] and N-doped Cu_2O.[53] The characteristic of additional sub-band absorptions suggests that the Fe dopants introduced new impurity levels or bands to the In_2S_3 and $MgIn_2S_4$ system. In order to probe the internal mechanism, the electronic band structure of host semiconductors and the Fe-doped compounds were investigated by using first-principles calculations.

In the case of Fe-substituted In_2S_3, the dopant atom may occupy the following four different positions according to the Wyckoff positions in the $I4_1/amd$ space group: 16h, 8c,

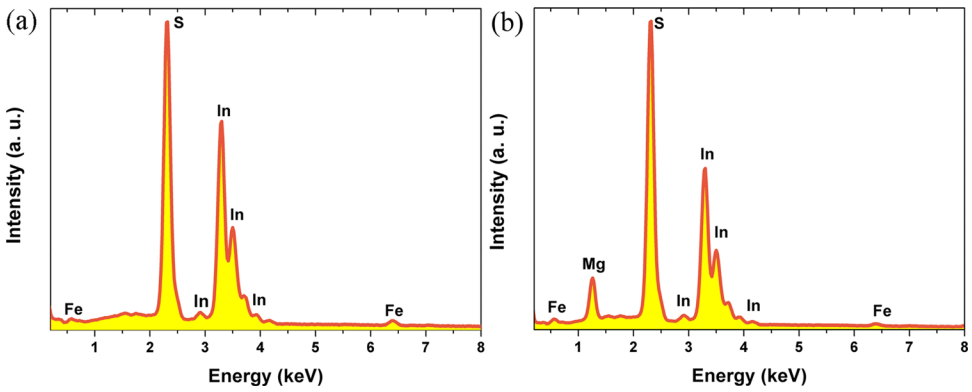

FIG. 3. The EDX of (a) $In_{1.9}Fe_{0.1}S_3$ and (b) $MgIn_{1.9}Fe_{0.1}S_4$, respectively.

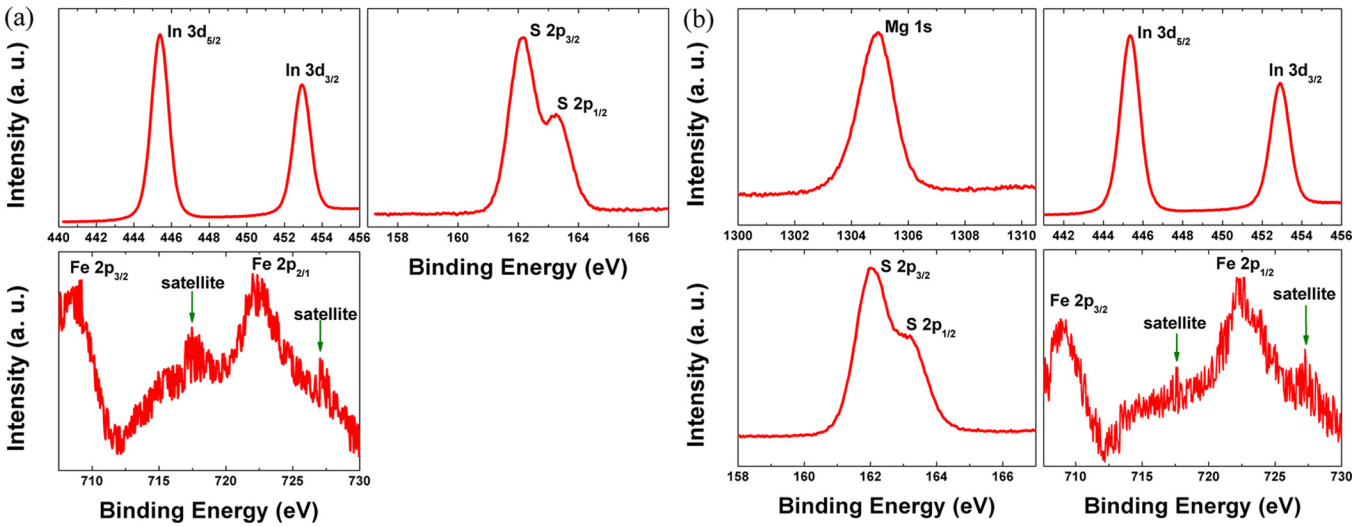

FIG. 4. The XPS spectra of (a) $In_{1.9}Fe_{0.1}S_3$ and (b) $MgIn_{1.9}Fe_{0.1}S_4$, respectively.

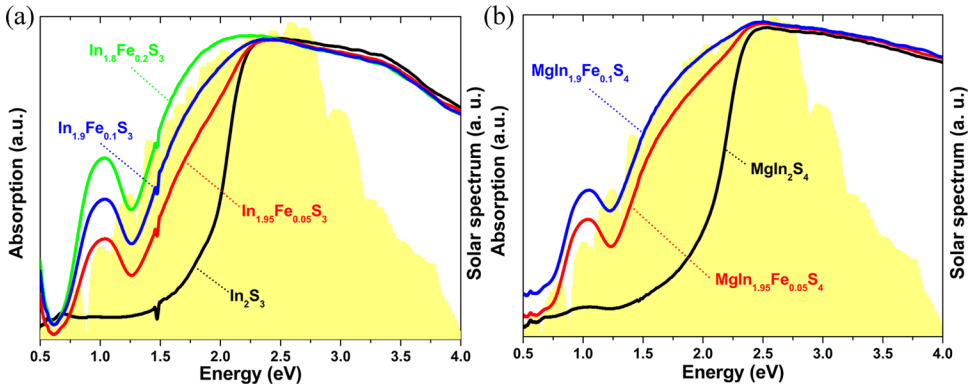

FIG. 5. The UV-Vis-NIR absorption spectra of the (a) $In_{2-x}Fe_xS_3$ and (b) $MgIn_{2-x}Fe_xS_4$, respectively.

TABLE II. The relative energy (MeV) of five Fe-doped In_2S_3 models ($In_{31}Fe_1S_{48}$).

	16h	8c	8e	$4a_{near}$	$4a_{far}$
Relative energy	0	251.6	680.7	1302.9	4140.7

8e, and 4a (the ordered vacant site). While the Fe atom occupies the 4a position, one In atom was removed from the crystal cell to maintain the stoichiometric ratio. Here, only two extreme situations were considered: the Fe atom and the removed In atom have the farthest ($4a_{far}$) and the nearest distance ($4a_{near}$), respectively. Thus, the structural optimization and energy calculations have been carried out for five models. Table II lists the relative energy of Fe-substituted five different In positions. In can be seen that the most stable position of Fe dopant is octahedral site 16h, and the occupation of ordered vacant site 4a is energetically unfavorable.

The calculated lattice parameters, crystal cell volume, and *M*-S (*M* = In, Fe) bonds of In_2S_3, $In_{31}Fe_1S_{48}$, $MgIn_2S_4$, and $Mg_8In_{15}Fe_1S_{32}$ are given in Table III. For the structural calculations of Fe-substituted In_2S_3, only the results of Fe atom at the Oh(16h) position are listed. The theoretical lattice parameters are in good agreement with the experimental and other theoretical values.[39,69–71] The lattices shrink slightly, and the Fe-S lengths are found to be shorter than the In-S bonds. The theoretical volumes decrease with respect to that of host semiconductors, which is consistent with our experimental results. Once the Fe substitutes the In position of In_2S_3, the lattice distortion occurred, where the lattice parameter *a* of tetragonal cell becomes unequal. However, in the case of Fe-doped $MgIn_2S_4$, the dopant does not bring any tetragonal distortion to the lattice.

The band structures of In_2S_3 and Fe-doped In_2S_3 at 16h position are plotted in Figure 6. For the pure In_2S_3 host semiconductor (Figure 6(a)), the calculated band gap between the conduction band minimum (CBM) and the valence band

TABLE III. The lattice parameter *a* (in Å) and atomic distance *d*(M-S) (in Å) for the pure semiconductors and the Fe-doped compounds, respectively. Other theoretical and experimental works are shown in brackets.

	a	*c*	V	*d*(M-S) bond
In_2S_3	7.56 (7.677,[a] 7.594)[b]	32.11 (32.755,[a] 32.352)[b]	1833.17	2.53–2.66 (In-S)
$In_{31}Fe_1S_{48}$	$a_1 = 7.54$, $a_2 = 7.53$	31.86	1808.56	2.25–2.34 (Fe-S)
$MgIn_2S_4$	10.66 (10.78,[c] 10.71)[d]		1210.28	2.59 (2.58,[c] 2.63)[d] (In-S)
$Mg_8In_{15}Fe_1S_{32}$	10.59		1187.62	2.29 (Fe-S)

[a]Theoretical work of Zhao *et al.*[69]
[b]Experimental result of Rampersadh *et al.*[70]
[c]Other theoretical work of Palacios *et al.*[39]
[d]Experimental result of Hahn *et al.*[71]

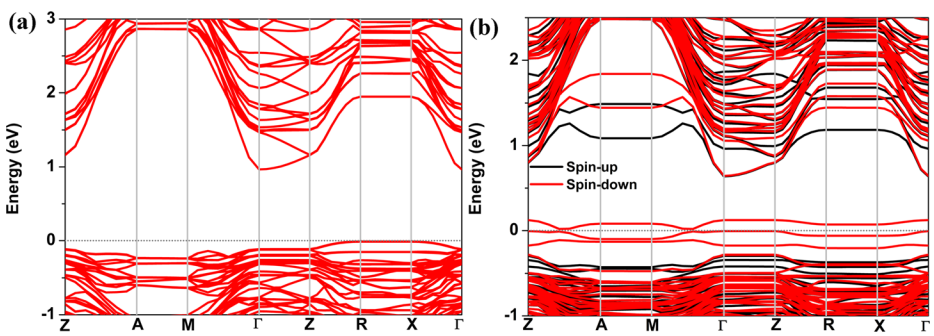

FIG. 6. The band structures of (a) In_2S_3 and (b) Fe-doped In_2S_3 at 16h position, respectively.

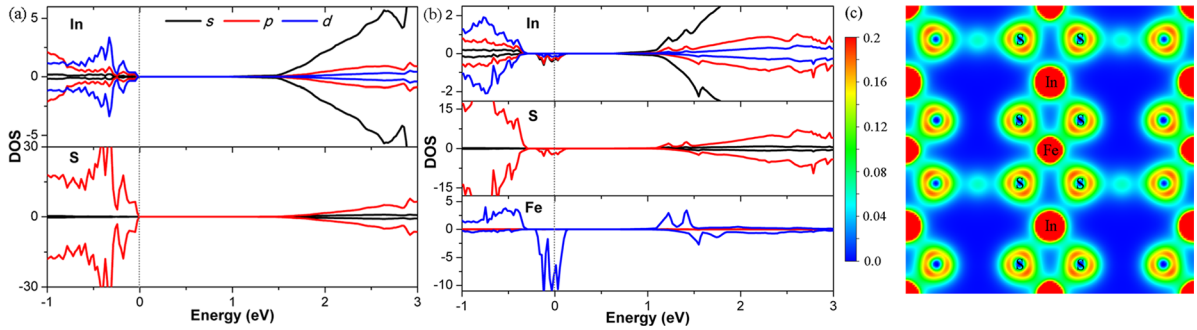

FIG. 7. The DOS of (a) In_2S_3 and (b) Fe-doped In_2S_3, respectively. (c) The charge density distribution on the Fe-S plane.

maximum (VBM) is 0.97 eV form the present LDA calculation, which is larger than the previously reported theoretical value 0.86 eV (Ref. 39) (using GGA-PW91 functional). Compared to the experimental value 1.85–2.2 eV,[55–57] it is a typical underestimation of gap in the DFT calculations due to the missing discontinuity in the exchange-correlation potential and the self-interaction error. The CBM is at the Γ point and the VBM at the R point, which indicate the In_2S_3 is an indirect semiconductor. From Figure 6(b), it can be seen that an isolated IB is introduced with the Fe-substitution. The spin-down IB is metallic which is crossed by the Fermi level. It should note that the calculated band gap *E*g of In_2S_3 cannot directly compare with the experimental value because the LDA approximation underestimated the values between the occupied and unoccupied states. Thus, the accurate positions of the IB cannot be determined in the present calculations. However, the IB character which caused by the Fe-dopant would not be affected by this underestimation because IB is metallic. Actually, the successes of DFT calculations in prediction IB materials have been reported in previous work although it underestimated the band gap, such as V-doped In_2S_3 (Ref. 47) or SnS_2 (Ref. 48) and Cr-doped $CuGaS_2$.[49]

In order to gain the nature of chemical bonding, the electronic DOS of In_2S_3 and Fe-doped In_2S_3 at 16h position are shown in Figure 7. For In_2S_3 (Figure 7(a)), the topmost of VB is mainly composed of S-3*p* states, whereas the In-5*s* and S-3*p* states nearly have the same contribution to the CBM. The metallic IB is mainly derived from the Fe-3*d* states and also some hybrid states of S-3*p* (Figure 7(b)). It shows that Fe impurity states play an important role in the IB-related optical transitions. Both below and above the Fermi level, the hybridization between Fe-3*d* states and S-3*p* states is strong. To further analyze the chemical bonding, the charge density distribution of Fe-doped In_2S_3 on the Fe-S plane is depicted in Figure 7(c). The contour lines are plotted from 0.0 to 0.2 e/Å^3. The large charge accumulation between Fe-S atoms and aspherical shape indicate the formation of covalent bonding between them. The In-S bond also shows the occurrence of covalent character. These results are in consistent with the DOS analysis, which shows the hybridization between the Fe (or In) and S atoms.

For the $MgIn_2S_4$, the obtained direct gap at the Γ point is 1.57 eV, which is agreement with the previously calculated result 1.65 eV (Figure 8(a)). Compared to the experimental values 2.1–2.28 eV,[58,59] the DFT underestimates the band

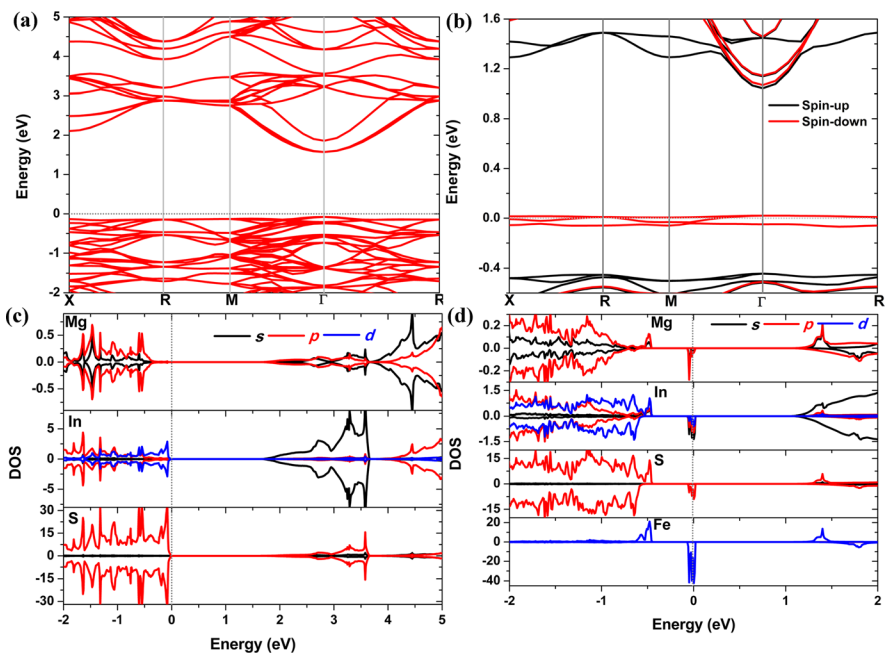

FIG. 8. The band structures of (a) $MgIn_2S_4$ and (b) Fe-doped $MgIn_2S_4$, respectively. The DOS of (c) $MgIn_2S_4$ and (d) Fe-doped $MgIn_2S_4$, respectively.

gap. From the calculated DOS in Figure 8(c), it is seen that the topmost of VB is mainly derived from the S 3*p* orbital, and the lowest conduction band is dominated by the S 3*p* and In 5*s* states. Above the Fermi level, the *s-p* hybridization between In and S is strong. The Mg 2*p* and 3*s* states are very weak in these regions. Figure 8(b) shows the band structure of Fe-doped $MgIn_2S_4$ system. An isolated metallic IB was formed in the gap with the Fe-substitution, which is composed of three energy bands. The IB is mainly derived from the Fe 3*d* states (Figure 8(d)). The hybridization of the Fe 3*d* and S 3*p* in entire region indicates the formation of strong covalent bonding between them.

Based on the theoretical analysis above, it is found that the IB in In_2S_3 and $MgIn_2S_4$ systems shares some common characteristics. This is mainly due to the Fe dopant substituted the octahedral position in In-S polyhedron. For the Fe-substituted the In-S tetrahedral position, the Fe dopant only introduced an empty IB into the band gap (e.g., Fe doped $CuInS_2$).[72] This means the coordination environment is the key factor in bringing different IB to the host semiconductor. The metallic IB could act as the steeping stone and provide some new ways to optical transition. Theoretically, the electrons are directly excited from the VB to the IB, from the IB to the CB, and also from the VB to the CB by absorbing photons, respectively. The enhanced absorption of solar energy would provide an opportunity to increase the photovoltaic efficiency.

IV. CONCLUSIONS

In summary, we have carried a combined experimental preparation, characterization and first-principles investigation the structure, electronic, and optical properties of Fe-doped In_2S_3 and $MgIn_2S_4$ systems. Two IB semiconductors with wide-spectrum solar absorption were demonstrated. It was found that the In_2S_3 undergoes a phase transition from the tetragonal β to disordered cubic α phase due to chemical disorder of Fe substitution. The Fe-substituted In_2S_3 and $MgIn_2S_4$ led to strong absorption in the full solar spectrum area which would be attractive for photovoltaic applications. From the results of electronic structure, the Fe substitutes the octahedral In position in indium thiospinels, introducing a partially intermediate band into the band gap. The Fe elements can provide very strong 3*d* IB DOS which would be benefit to the photons absorption and IB-related optical transitions. The Fe substitute at the octahedral In position is energetically favorable, and hence it is beneficial to the experimental synthesis of stable compound with a high dopant concentration. Moreover, the fabrication of In_2S_3 thin film is mature, which seems to be a promising host semiconductor for the IBSC. These advantages indicate the Fe-doped indium thiospinels are potential candidates as the IB material for next photovoltaic devices.

ACKNOWLEDGMENTS

This work was supported by the National 863 Program of China (Grant No. 2011AA050505), NSF of China (Grant Nos. 91122034, 51202274, 51125006, 51102263, 61076062, and 21101164), STC of Shanghai (Grant No. 10JC1415800), and Innovation Project of SICCAS (Grant No. Y23ZC6160G).

[1]M. J. Keevers and M. A. Green, J. Appl. Phys. **75**, 4022 (1994).
[2]M. A. Green, Prog. Photovoltaics **9**, 123 (2001).
[3]M. A. Green, Prog. Photovoltaics **9**, 137 (2001).
[4]G. Beaucarne, A. S. Brown, M. J. Keevers, R. Corkish, and M. A. Green, Prog. Photovoltaics **10**, 345 (2002).
[5]W. Shockley and H. J. Queisser, J. Appl. Phys. **32**, 510 (1961).
[6]A. D. Vos, J. Phys. D: Appl. Phys. **13**, 839 (1980).
[7]A. Luque and A. Martí, Phys. Rev. Lett. **78**, 5014 (1997).
[8]T. Nozawa and Y. Arakawa, Appl. Phys. Lett. **98**, 171108 (2011).
[9]A. Luque and A. Martí, Nat. Photonics **5**, 137 (2011).
[10]A. Luque, A. Martí, C. Stanley, N. López, L. Cuadra, D. Zhou, J. L. Pearson, and A. McKee, J. Appl. Phys. **96**, 903 (2004).
[11]A. Marti, E. Antolin, C. R. Stanley, C. D. Farmer, N. López, P. Díaz, E. Cánovas, P. G. Linares, and A. Luque, Phys. Rev. Lett. **97**, 247701 (2006).
[12]W. Shan, W. Walukiewicz, J. W. Ager III, E. E. Haller, J. F. Geisz, D. J. Friedman, J. M. Olson, and S. R. Kurtz, Phys. Rev. Lett. **82**, 1221 (1999).
[13]K. M. Yu, W. Walukiewicz, J. Wu, W. Shan, J. W. Beeman, M. A. Scarpulla, O. D. Dubon, and P. Becla, Phys. Rev. Lett. **91**, 246403 (2003).
[14]E. D. Jones, N. A. Modine, A. A. Allerman, S. R. Kurtz, A. F. Wright, S. T. Tozer, and X. Wei, Phys. Rev. B **60**, 4430 (1999).
[15]T. Mattila, S. H. Wei, and A. Zunger, Phys. Rev. B **60**, 11245 (1999).
[16]J. Li, P. Carrier, S. H. Wei, S. S. Li, and J. B. Xia, Phys. Rev. Lett. **96**, 35505 (2006).
[17]A. Janotti, P. Reunchan, S. Limpijumnong, and C. G. Van de Walle, Phys. Rev. Lett. **100**, 045505 (2008).
[18]H. X. Deng, J. Li, S. S. Li, H. Peng, J. B. Xia, L. W. Wang, and S. H. Wei, Phys. Rev. B **82**, 193204 (2010).
[19]V. Virkkala, V. Havu, F. Tuomisto, and M. J. Puska, Phys. Rev. B **85**, 085134 (2012).
[20]J. Li and S. H. Wei, Phys. Rev. B **73**, 041201 (2006).
[21]C. Tablero, A. Martí, and A. Luque, Appl. Phys. Lett. **96**, 121104 (2010).
[22]C. Tablero, Comput. Mater. Sci. **49**, 368 (2010).
[23]N. Shtinkov, P. Desjardins, and R. A. Masut, Phys. Rev. B **67**, 081202 (2003).
[24]K. Kim and A. Zunger, Phys. Rev. Lett. **86**, 2609 (2001).
[25]P. R. C. Kent and A. Zunger, Phys. Rev. B **64**, 115208 (2001).
[26]A. Lindsay and E. P. O'Reilly, Solid State Commun. **112**, 443 (1999).
[27]N. López, L. A. Reichertz, K. M. Yu, K. Campman, and W. Walukiewicz, Phys. Rev. Lett. **106**, 028701 (2011).
[28]A. Luque and A. Martí, Adv. Mater. **22**, 160 (2010).
[29]T. Tanaka, S. Kusaba, T. Mochinaga, K. Saito, Q. Guo, M. Nishio, K. M. Yu, and W. Walukiewicz, Appl. Phys. Lett. **100**, 011905 (2012).
[30]P. Wahnón and C. Tablero, Phys. Rev. B **65**, 165115 (2002).
[31]C. Tablero and P. Wahnón, Appl. Phys. Lett. **82**, 151 (2003).
[32]C. Tablero, Phys. Rev. B **72**, 035213 (2005).
[33]P. Palacios, J. J. Fernández, K. Sánchez, J. C. Conesa, and P. Wahnón, Phys. Rev. B **73**, 085206 (2006).
[34]P. Palacios, K. Sánchez, J. C. Conesa, and P. Wahnón, Phys. Status Solidi A **203**, 1395 (2006).
[35]P. Palacios, K. Sánchez, J. C. Conesa, J. J. Fernández, and P. Wahnón, Thin Solid Films **515**, 6280 (2007).
[36]C. Tablero, Phys. Rev. B **74**, 195203 (2006).
[37]C. Tablero, Sol. Energy Mater. Sol. Cells **90**, 588 (2006).
[38]C. Tablero, Comput. Mater. Sci. **37**, 483 (2006).
[39]P. Palacios, I. Aguilera, K. Sánchez, J. C. Conesa, and P. Wahnón, Phys. Rev. Lett. **101**, 046403 (2008).
[40]I. Aguilera, P. Palacios, K. Sánchez, and P. Wahnón, Phys. Rev. B **81**, 075206 (2010).
[41]P. Olsson, C. Domain, and J.-F. Guillemoles, Phys. Rev. Lett. **102**, 227204 (2009).
[42]K. Sánchez, I. Aguilera, P. Palacios, and P. Wahnón, Phys. Rev. B **79**, 165203 (2009).
[43]K. Sánchez, I. Aguilera, P. Palacios, and P. Wahnón, Phys. Rev. B **82**, 165201 (2010).
[44]C. Tablero, "Photovoltaic application of O-doped Wittichenite-Cu 3 BiS 3: from microscopic properties to maximum efficiencies," Prog. Photovoltaics (to be published).
[45]C. Tablero, Sol. Energy Mater. Sol. Cells **104**, 180 (2012).
[46]C. Tablero, J. Phys. Chem. C **116**, 23224 (2012).

[47]R. Lucena, I. Aguilera, P. Palacios, P. Wahnón, and J. C. Conesa, Chem. Mater. **20**, 5125 (2008).
[48]P. Wahnón, J. C. Conesa, P. Palacios, R. Lucena, I. Aguilera, Y. Seminovski, and F. Fresno, Phys. Chem. Chem. Phys. **13**, 20401 (2011).
[49]P. Chen, M. Qin, H. Chen, C. Yang, Y. Wang, and F. Huang, "Cr incorporation in $CuGaS_2$ chalcopyrite: A new intermediate-band photovoltaic material with wide-spectrum solar absorption," Phys. Status Solidi A (to be published).
[50]M. S. Qin, F. Q. Huang, and P. Chen, AMM **148**, 1558 (2012).
[51]C. Yang, M. Qin, Y. Wang, D. Wan, F. Huang, and J. Lin, "Observation of an Intermediate Band in Sn-doped Chalcopyrites with Wide-spectrum Solar Response," Sci. Rep. (to be published).
[52]C. H. Ho, J. Mater. Chem. **21**, 10518 (2011).
[53]C. Malerba, C. L. Azanza Ricardo, M. D'Incau, F. Biccari, P. Scardi, and A. Mittiga, Sol. Energy Mater. Sol. Cells **105**, 192 (2012).
[54]D. Braunger, D. Hariskos, T. Walter, and H. W. Schock, Sol. Energy Mater. Sol. Cells **40**, 97 (1996).
[55]M. G. Sandoval-Paz, M. Sotelo-Lerma, J. J. Valenzuela-Jáuregui, M. Flores-Acosta, and R. Ramírez-Bon, Thin Solid Films **472**, 5 (2005).
[56]N. Barreau, A. Mokrani, F. Couzinié-Devy, and J. Kessler, Thin Solid Films **517**, 2316 (2009).
[57]W. T. Kim and C. D. Kim, J. Appl. Phys. **60**, 2631 (1986).
[58]M. Wakaki, O. Shintani, T. Ogawa, and T. Arai, Jpn. J. Appl. Phys. **19**, 255 (1980).
[59]P. M. Sirimanne, N. Sonoyama, and T. Sakata, J. Solid State Chem. **154**, 476 (2000).
[60]G. Kresse and J. Furthmüller, Comput. Mater. Sci. **6**, 15 (1996).
[61]G. Kresse and J. Furthmüller, Phys. Rev. B **54**, 11169 (1996).
[62]P. E. Blöchl, Phys. Rev. B **50**, 17953 (1994).
[63]R. Diehl and R. Nitsche, J. Cryst. Growth **28**, 306 (1975).
[64]S. Gorai, P. Guha, D. Ganguli, and S. Chaudhuri, Mater. Chem. Phys. **82**, 974 (2003).
[65]A. Lafond, X. Rocquefelte, M. Paris, C. Guillot-Deudon, and V. Jouenne, Chem. Mater. **23**, 5168 (2011).
[66]R. D. Shannon, Acta Cryst. A **32**, 751 (1976).
[67]T. Yamashita and P. Hayes, Appl. Surf. Sci. **254**, 2441 (2008).
[68]P. Kubelka, J. Opt. Soc. Am. **38**, 448 (1948).
[69]Z. Zhao, Y. Cao, J. Yi, X. He, C. Ma, and J. Qiu, ChemPhysChem. **13**, 1551 (2012).
[70]N. S. Rampersadh, A. M. Venter, and D. G. Billing, Physica B **350**, E383 (2004).
[71]H. Hahn and W. Klingler, Z. Anorg. Allg. Chem. **263**, 177 (1950).
[72]C. Tablero, Chem. Phys. Lett. **499**, 75 (2010).